On the time lag between sea-level rise and basin infilling at tidal inlets

Ranasinghe, Roshanka; Wang, Zheng Bing; Bamunawala, Janaka; Duong, Trang Minh

DOI
10.1038/s41598-025-86699-0

Publication date
2025

Document Version
Final published version

Published in
Scientific Reports

scientific reports

Check for updates

OPEN

On the time lag between sea-level rise and basin infilling at tidal inlets

Roshanka Ranasinghe[1,2,3]✉, Zheng Bing Wang[2,4], Janaka Bamunawala[5] & Trang Minh Duong[1,2,3]

Tidal inlets are a common feature along the world's coastline. Inlet-adjacent coastlines have for millennia supported communities and livelihoods, and therefore, projected climate change driven variations in catchment-estuary-coast (CEC) system drivers (e.g., sea-level rise (SLR)) are likely to lead to substantial socio-economic impacts. One important SLR-driven process that affects inlet-adjacent shoreline change is basin-infilling (i.e., sediment import to the estuary from the coast to satisfy the SLR-driven increase of estuarine accommodation space). Due to the slow morphological response to hydrodynamic forcing, however, there is a time lag between basin infilling and SLR, which, in numerical models that simulate century-scale evolution of CEC systems, is represented by a basin infilling lag factor (*M*). To date, an indicative *M* value has only been derived for small tidal inlet systems (*M* ~0.5), and due to the lack of *M* estimates for larger systems, studies have been using *M* ~0.5 indiscriminately. Here, for the first time, we derive indicative *M* values for small, medium, and large tidal inlet systems (*M* ~0.5, ~0.25 and ~0.15 respectively) via analytical considerations. Subsequently, to investigate the consequences of using sub-optimal *M* values on twenty-first century projections of inlet-adjacent shoreline change, we apply a probabilistic, reduced complexity model (*G-SMIC*), under four IPCC AR6 climate scenarios, to three CEC systems representing small, medium and large systems. Results show that, in general, shoreline change projections are substantially lower(higher) when *M* values smaller(larger) than the indicative *M* for a given system are used. When smaller-than-optimal *M* values (0.25 and 0.15) are used for the small tidal inlet, both mid- and end-century shoreline retreats are under-estimated by 50–75% (across the four climate scenarios), relative to projections obtained with the optimal *M* value. For the medium-sized inlet, shoreline retreats for both future periods are over-estimated by ~100% with the larger-than-optimal *M* value of 0.5, while they are under-estimated by ~40–75% (across climate scenarios) with the smaller-than-optimal *M* value of 0.15. When the two higher-than-optimal *M* values (0.25 and 0.5) are used for the large tidal inlet system, shoreline retreat is over-estimated by ~ 65–240% (across climate scenarios) for both future periods. In terms of absolute values, these under/over-estimations increase in time and with the severity of emission scenario.

Estuaries connected to the ocean via a narrow inlet channel, often referred to simply as "tidal inlets", can be commonly found all over the world[1–9]. These inlets come in different types, shapes and sizes[6], and in general, inlet-adjacent coastlines have supported many human activities such as fishing, sand mining, navigation, and waterfront developments, to name a few[2,8,10,11]. As such, inlet-interrupted coasts have for centuries attracted human settlements, making them highly sought after regions[11–13]. Any changes to the inlet-coast system that impacts on such human activities would, therefore, lead to heavy socio-economic consequences and, in some cases, may even threaten the safety of coastal communities[8–11].

It is now well understood that the stability of tidal inlets and adjacent coastlines is a function of both oceanic (e.g., change in mean sea level) and terrestrial (e.g., change in fluvial sediment supply) processes[8,9,11,13]. Climate change, however, is projected to affect almost all key inlet system drivers, such as mean sea level, riverflow, ocean waves, and storm surges[6,8–10]. In fact, several impact assessments have shown that climate change-driven impacts at inlet-coast systems are all but inevitable over the twenty-first century[8,9,13–22].

One of the key processes governing tidal inlet response to especially sea-level rise (SLR) is the process known as basin infilling[11,23], which is the focus of this contribution. When the mean sea level increases, the estuary volume will also increase by a certain amount (i.e., accommodation space). To maintain its initial equilibrium

[1]Department of Coastal and Urban Risk & Resilience, IHE Delft Institute for Water Education, P.O. Box 3015, 2601 DA Delft, The Netherlands. [2]Deltares, P.O. Box 177, 2600 MH Delft, The Netherlands. [3]Water Engineering and Management, University of Twente, P.O. Box 217, 7500 AE Enschede, The Netherlands. [4]Faculty of Civil Engineering and Geosciences, Delft University of Technology, P.O. Box 5048, 2600 GA Delft, The Netherlands. [5]Department of Civil and Environmental Engineering, Graduate School of Engineering, Tohoku University, Sendai, Japan. ✉email: r.ranasinghe@un-ihe.org

state, the estuary will then strive to import a sediment volume equal to this SLR-driven increase in estuary volume. This is the process known as SLR-driven basin infilling. However, as the time scales associated with hydrodynamic forcing and morphological response are different, there will be a potential time lag between SLR and basin infilling. Through analytical considerations, Ranasinghe et al.[11] showed that, for small tidal inlets (defined as systems with estuary surface areas of around 50–100 km^2), this time lag is approximately 50% (i.e., at any given time, the SLR-driven accommodation space in an estuary will only be half filled up by basin infilling). This simplification has been used extensively in the reduced complexity model *SMIC*[11] and its successor *G-SMIC*[8,9,21]. However, as stated in Ranasinghe et al.[11], this time lag of 50%, represented in the aforementioned reduced complexity models by a so-called 'lag-factor' M equal to 0.5 in the term representing basin infilling, is valid only for small tidal inlets. In this contribution, starting with the analytical considerations in Ranasinghe et al.[11], we explore how M might vary for larger tidal inlets. In this regard, two additional cases are considered: medium and large inlets, with the respective surface areas twice and four times that typical of small tidal inlets. Subsequently, through applications of *G-SMIC* to systems representing small, medium and large inlets with different M values, we investigate the potential under/over-estimation of future shoreline change along the inlet-adjacent coast that could result from using inappropriate M values in computations. Please see Methods for more details on the analytical derivation for M, a brief description of *G-SMIC* and its implementation in this study.

Results

Lag factor *M* for different tidal inlets

Using analytical methods (fully described in Methods), the following M values are obtained for different tidal inlet systems:

- $M \sim 0.5$ for Small tidal inlets (~ 50 km$^2 < A_B < 100$ km^2)
- $M \sim 0.25$ for Medium-sized tidal inlets (~ 100 km$^2 < A_B < 200$ km^2); and
- $M \sim 0.15$ for Large tidal inlets (~ 200 km$^2 < A_B < 400$ km^2).

Where, A_B is the horizontal basin surface area. The medium and large tidal inlet classes here are based on the estuary data base used by Bamunawala et al.[21].

Essentially, the above results imply that larger systems take much longer than smaller systems to morphologically respond to SLR, which is in line with previous assertions[4,23–27].

The impact of using inappropriate *M* values in shoreline change assessments

Here, we present the *G-SMIC* projected inlet-adjacent shoreline changes by the middle and end of the twenty-first century under four IPCC AR6 climate scenarios (SSP1-2.6, SSP2-4.5, SSP3-7.0, and SSP5-8.5), at all three types of inlet systems, with all three M values derived above. The representative systems considered here, and their key system characteristics are shown in (Fig. 1 and Table 1).

Table 2 shows the decadal averaged median (i.e., 50th percentile) projections of shoreline positions (Δx_{sv}) at the selected three case studies for the four considered climate scenarios for mid-century (2056–2065) and end-century (2091–2100) periods. These median values are extracted from fully probabilistic *G-SMIC* projections. For the sake of completeness, decadal averaged 10th, 50th, and 90th percentile values of sediment exchange volume between the estuary and the coast (ΔV_T) during the mid-century (2056–2065) and end-century (2091–2100) periods are shown in Supplementary Tables S1, S2, while the consequent variations in shoreline positions (Δx_{sv}) are shown in Supplementary Tables S3, S4, respectively.

For all three inlet systems, in general, the results show that projected future variations in shoreline position (Δx_{sv}, in m) are substantially lower(higher) when M values smaller (larger) than the indicative M value for the system type are used, under all climate scenarios and for both future time periods. For the small inlet system (indicative $M \sim 0.5$), across the four considered climate scenarios, shoreline retreat is under-estimated (relative to the shoreline retreat projected with the appropriate indicative M value of 0.5) by between 50–75% for both mid and end-twenty-first century when using the two smaller M values (0.25 and 0.15). In terms of absolute values, the under-estimation of shoreline retreat for this system can be up to ~ 25 m for mid-century and as high as ~ 50 m for end-century. For the medium-sized inlet system (indicative $M \sim 0.25$), shoreline retreat is over-estimated by $\sim 100\%$ under all climate scenarios and for both future time periods (over-estimations of ~ 10 m–15 m and ~ 20 m–35 m for mid and end-century, respectively) when the higher-than-optimal M value of 0.5 is used. Conversely, when the lower-than-optimal M value of 0.15 is used at the medium-sized inlet system, shoreline change is under-estimated by 40–75% across the considered climate scenarios for both future periods (under-estimations of ~ 5 m and 10–15 m for mid and end-century, respectively). When the two higher-than-optimal M values are used for the large tidal inlet system (optimal $M \sim 0.15$), shoreline retreat is over-estimated by ~ 65–240% across all climate scenarios and for both future time periods (over-estimations of up to ~ 15–75 m and up to ~ 30–165 m for mid and end-century, respectively). It is also noteworthy that, in terms of absolute values, all these under/over-estimations increase in time and with the severity of emission scenario.

It should be noted that all the shoreline variations presented in Table 2 and Supplementary Tables are only due to projected changes in sediment volume exchange (ΔV_T). In addition to this, these systems will inevitably experience an additional SLR-driven coastal recession due to the so-called Bruun effect[28], which is not included in the results presented in this study. Furthermore, here, we do not consider any significant changes in river catchments (such as dam removal or construction of new dams) that might substantially change the overall sediment exchange volume and the consequent shoreline position change.

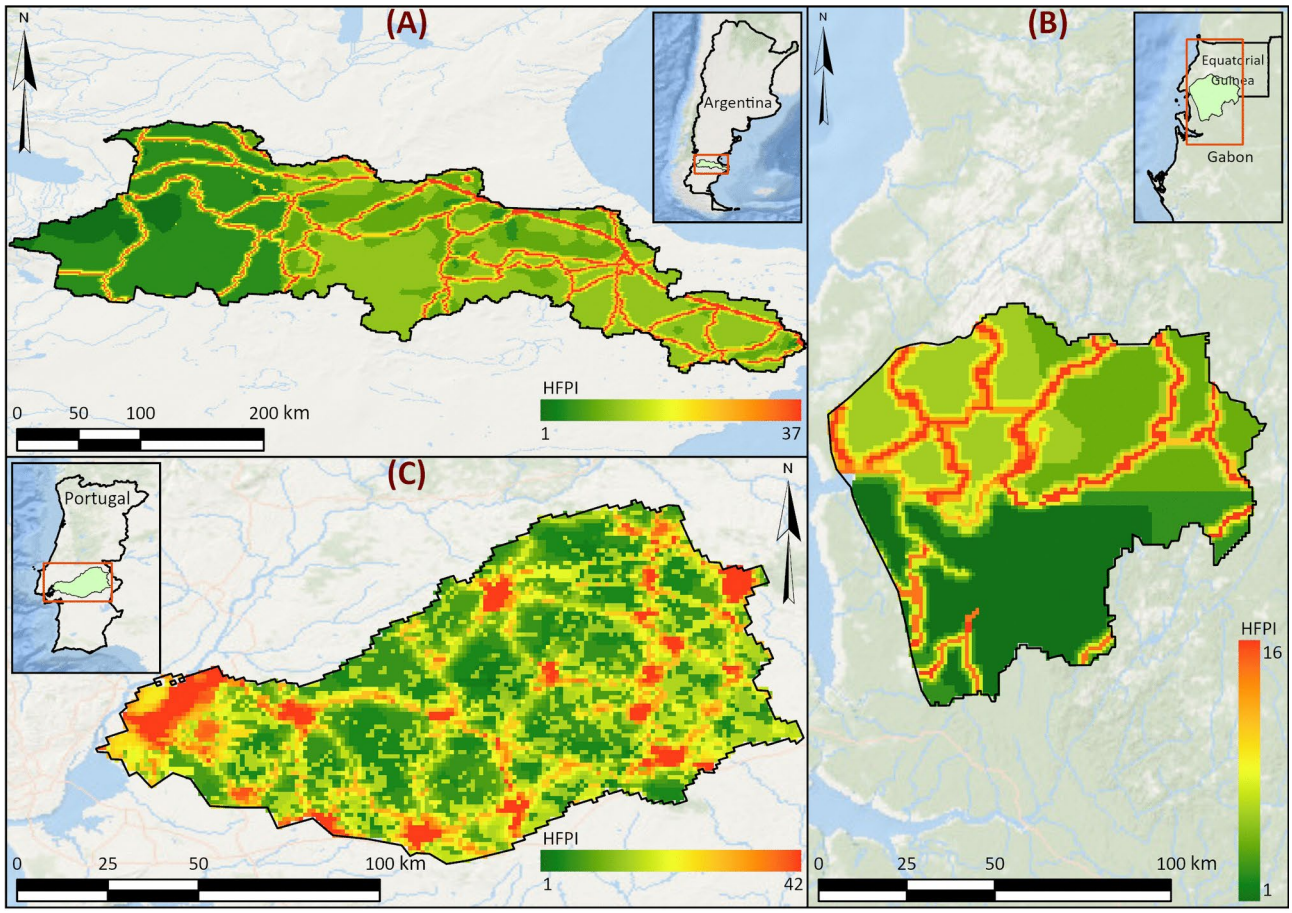

Fig. 1. Location, watershed, and Human FootPrint Index (HFPI) of the case studies: (**A**) Rio Deseado (small system), (**B**) Muni (medium system), and (**C**) Lisboa (large system). HFPI data were obtained from https://doi.org/10.7927/H46T0JQ4. Figure created with ArcGIS Pro, ver 3.3.1 (https://www.esri.com/en-us/arcgis/products/arcgis-pro/overview).

Parameter	Rio Deseado, Argentina *(small tidal inlet)*	Muni, Equatorial Guinea *(medium-sized tidal inlet)*	Lisboa, Portugal *(large tidal inlet)*
Basin surface area (A_B in km^2)	90	185	320
River catchment area (A in km^2)	38,743	7995	8022
Basin volume (V in $\times 10^6 m^3$)	166.3	341.8	591.2
Catchment relief (R in km)	2.4	1.15	0.98
Catchment lithology factor (L_c)	1	0.5	1.5
Anthropogenic factor (E_h)	0.41	0.396	0.64
Mean ebb-tidal prism (P in $\times 10^6 m^3$)	682.2	482.9	1340.8
Depth of closure (DoC in m)	15	20	15
Length of inlet-affected coastline (km)	30	50	35

Table 1. Properties of the selected tidal inlet systems (see methods for data sources).

Conclusions

This study investigated the time lag between SLR and basin infilling; both being important processes that affect inlet-adjacent shoreline change. In numerical models that simulate century-scale evolution of tidal inlets this time lag is represented by a basin infilling lag factor (M). However, an indicative M value has only been derived for small tidal inlet systems ($M \sim 0.5$) to date, which has resulted in this one value being used indiscriminately for larger inlet systems. In this study, physics based analytical methods were used to derive M values for different tidal inlet systems with the following results:

Tidal-Inlet system	Lag factor (M)	Decadal-averaged projections of shoreline position change (Δx_{sv} in m) for the 2056–2065 period			
		SSP1-2.6	SSP2-4.5	SSP3-7.0	SSP5-8.5
Rio Deseado (small)	0.50	**−25 (–)**	**−28 (–)**	**−30 (–)**	**−33 (–)**
	0.25	−12 (−52%)	−14 (−51%)	−15 (−52%)	−16 (−51%)
	0.15	−7 (−73%)	−8 (−72%)	−8 (−72%)	−9 (−72%)
Muni (medium)	0.50	−24 (100%)	−27 (93%)	−29 (93%)	−32 (100%)
	0.25	**−12 (–)**	**−14 (–)**	**−15 (–)**	**−16 (–)**
	0.15	−7 (−42%)	−8 (−75%)	−9 (−40%)	−10 (−38%)
Lisboa (large)	0.50	−79 (235%)	−88 (236%)	−96(235%)	−104 (234%)
	0.25	−39 (67%)	−44 (67%)	−48 (67%)	−52 (67%)
	0.15	**−24 (–)**	**−26 (–)**	**−29 (–)**	**−31 (–)**
		Decadal-averaged projections of shoreline position change (Δx_{sv} in m) for the 2091–2100 period			
Rio Deseado (small)	**0.50**	**−43 (–)**	**−54 (–)**	**−64 (–)**	**−73 (–)**
	0.25	−20 (−53%)	−25 (−53%)	−30 (−53%)	−35 (−52%)
	0.15	−11 (−75%)	−14 (−74%)	−16 (−74%)	−19 (−74%)
Muni (medium)	0.50	−42 (100%)	−53 (104%)	−63 (97%)	−71 (97%)
	0.25	**−21 (–)**	**−26 (–)**	**−32 (–)**	**−36 (–)**
	0.15	−13 (−38%)	−16 (−63%)	−19 (−41%)	−22 (−39%)
Lisboa (large)	0.50	−139 (240%)	−173 (239%)	−207 (239%)	−234 (237%)
	0.25	−69 (68%)	−86 (68%)	−103 (69%)	−116 (68%)
	0.15	**−41 (–)**	**−51 (–)**	**−61 (–)**	**−69 (–)**

Table 2. Median (i.e., 50th percentile) projections of time-averaged shoreline position change (Δx_{sv}) relative to present-day at the selected case study locations under four IPCC AR6 climate scenarios for mid and end-twenty-first century periods. Negative values indicate shoreline retreat. For each system type, bold numbers indicate the projections obtained when using the indicative basin infilling lag factor (M) for that system, while the non-bold numbers show the result when M values other than the indicative M value are used for a given system. The % values within brackets indicate the % difference between each projection and the projection using the indicative M value (negative % change indicates an under-prediction relative to the projection with the indicative M value for the system).

- $M \sim 0.5$ for Small tidal inlets ($\sim 50\ km^2 < A_B < 100\ km^2$)
- $M \sim 0.25$ for Medium-sized tidal inlets ($\sim 100\ km^2 < A_B < 200\ km^2$); and
- $M \sim 0.15$ for Large tidal inlets ($\sim 200\ km^2 < A_B < 400\ km^2$).

where, A_B is the horizontal basin surface area.

The consequences of using sub-optimal M values on twenty-first century projections of inlet-adjacent shoreline change were investigated through the application of the probabilistic, physics-based, reduced complexity model (*G-SMIC*), under SSP1-2.6, SSP2-4.5, SSP3-7.0, and SSP5-8.5, to three tidal inlet systems representing small, medium, and large systems. Results showed that, in general, shoreline change projections are substantially lower(higher) when M values smaller(larger) than the indicative M for a given system are used, under all climate scenarios considered and for both mid- and end-twenty-first century periods. More specifically, for the small inlet system (indicative $M \sim 0.5$), when smaller-than-optimal M values (0.25 and 0.15) are used, both mid- and end-century shoreline retreats are under-estimated by 50–75% across the four climate scenarios (relative to the shoreline retreat projected with the appropriate indicative M value of 0.5). In the case of the medium-sized inlet, across the four climate scenarios, shoreline retreats are over-estimated by ~ 100% for both future periods when the larger-than-optimal M value of 0.5 is used, while they are under-estimated by ~ 40–75% when the smaller-than-optimal M value of 0.15 is used. For the large tidal inlet system, shoreline retreat is over-estimated by ~ 65–240% (across the four climate scenarios) for both future periods when the two higher-than-optimal M values (0.25 and 0.5) are used. The absolute values (i.e. meters instead of percentages) of these under/over-estimations increase in time and with the severity of emission scenario.

Methods

Analytical solution for the basin infilling lag factor *M*

For the sake of completeness, here we first reproduce the derivation of $M \sim 0.5$ for small tidal inlets presented in Ranasinghe et al.[11] and then expand the analysis to larger inlets.

The derivation of the basin infilling lag factor M presented here is based on the *ASMITA* model[24]. *ASMITA* conserves sediment within an inlet system (comprising ebb delta, channel, and basin) and the 'outside world' (which represents the adjacent nearshore area). *ASMITA* has two basic assumptions: (1) sediment exchange between the inlet system elements and with the 'outside world' drives morphological interaction between the three system elements, and (2) the 'outside world' is always in a state of equilibrium. Thus, when, for example,

SLR perturbs the system, the three elements and the outside world interact in such a way that each of the three system elements evolves towards a dynamic equilibrium state. For the M factor derivation here, we use the simplified single-element version of ASMITA presented by Van Goor et al.[25], given by:

$$\frac{\mathrm{d}V}{\mathrm{d}t} = \frac{V_\mathrm{B} - V}{T} + A_\mathrm{B} R \tag{1}$$

where, V is the wet volume of the basin below the changing sea level (in m^3), t is time (in years), V_B is the equilibrium volume in the absence of sea-level change (taken as the present-day basin volume; m^3); T is the morphological time scale of the inlet/basin system (in years), A_B is the horizontal surface area of the basin (in m^2), and R is the rate of SLR (in m/year).

The first term on the right-hand side of [1] represents the basin volume change due to erosion, and the second term on the right-hand side represents the SLR-driven change of the basin volume. Therefore, the sediment import rate into the basin is given by:

$$Q_\mathrm{Bi} = \frac{V - V_\mathrm{B}}{T} \tag{2}$$

If R is assumed to be more or less a constant, the solution of equation [1] is:

$$V = (V_0 - V_e)\, e^{-\left(\frac{t}{T}\right)} + V_e \tag{3}$$

where, V_0 is the initial value of V (i.e., $V(t=0)$), and V_e represents the dynamic equilibrium volume (i.e., the basin volume that would result after a long time of sea-level rise at a constant rate R).

The rate of volume change should be zero (i.e., ${}^{dV}/_{dt} = 0$) when dynamic equilibrium is achieved, and thus by substituting $V = V_\mathrm{e}$ in [1]:

$$V_\mathrm{e} = V_\mathrm{B} + A_\mathrm{B} R T \tag{4}$$

Assuming that the rate of sea-level rise increases from a rate R_1 to R_2 at $t=0$ (e.g., at the beginning of the twenty-first century), the solution becomes:

$$V = (V_{\mathrm{e}1} - V_{\mathrm{e}2})\, e^{-\left(\frac{t}{T}\right)} + V_{\mathrm{e}2} = A_\mathrm{B} T\,(R_1 - R_2)\, e^{-\left(\frac{t}{T}\right)} + V_\mathrm{B} + A_\mathrm{B} T R_2 \tag{5}$$

By substituting [5] for V in [2], the sediment import into the basin (or SLR-induced basin infilling) is given by:

$$Q_\mathrm{Bi} = A_\mathrm{B}\,(R_1 - R_2)\, e^{-\left(\frac{t}{T}\right)} + A_\mathrm{B} R_2 \tag{6}$$

The total basin infilling volume during a given time period (i.e., $t=t_1$ to $t=t_2$) can be calculated by integrating [6] within the limits of t as:

$$A_\mathrm{B} T\,(R_1 - R_2)\left[e^{-\left(\frac{t_1}{T}\right)} - e^{-\left(\frac{t_2}{T}\right)}\right] + A_\mathrm{B} R_2\,(t_2 - t_1) \tag{7}$$

By definition, the basin infilling volume is equal to the lag factor (M) multiplied by the accommodation space due to SLR:

$$M \Delta S A_\mathrm{B} = A_\mathrm{B} T\,(R_1 - R_2)\left[e^{-\left(\frac{t_1}{T}\right)} - e^{-\left(\frac{t_2}{T}\right)}\right] + A_\mathrm{B} R_2\,(t_2 - t_1) \tag{8}$$

As SLR over the twentieth century has been very slow (Fox-Kemper et al.[29] report an average rate global mean sea level change of 1.35 [0.78 to 1.92, *very likely* range] mm yr^{-1}), R_1 can be assumed to be zero, which reduces [8] to:

$$M \Delta S = R_2\,(t_2 - t_1) + T R_2\left[e^{-\left(\frac{t_2}{T}\right)} - e^{-\left(\frac{t_1}{T}\right)}\right] \tag{9}$$

Following Stive and Wang[23], the Morphological time scale T can be defined as:

$$T = \frac{V_e}{n C_\mathrm{E}}\left[\frac{1}{w_\mathrm{s} A_\mathrm{B}} + \frac{1}{\delta}\right] \tag{10}$$

where, n is an empirical coefficient between 3 and 5[11], C_E is the representative (long-term average) volumetric sediment concentration in the system, w_s is the vertical exchange velocity of sediment (in m/s), and horizontal

exchange coefficient $\delta = \frac{DA_c}{L}$, in which D is the diffusion coefficient (in m^2/s), A_c is the inlet channel cross-sectional area (in m^2), and L is a length measurement (in m), representing the distance between the inside and outside of the basin.

Assuming typical values of the above variables for small inlet systems with $A_B = 75 \times 10^6\ m^2$ ($n = 5$; $C_E = 3.14 \times 10^{-4}$; $V_e = 200 \times 10^6\ m^3$; $w_s = 0.001$ m/s; $D = 200\ m^2/s$, $A_c = 2{,}000\ m^2$, and $L = 10{,}000$ m), the morphological time scale T is estimated as ~ 100 years. Now, substituting $t_1 = 0$; $t_2 = 100$ years, $T = 100$ years, and $\Delta S = R_2 t_2$ (by assuming a linear rate of SLR) in [9] yield $M = 0.37$, rounded off as ~ 0.5.

In order to extend the lag factor analysis to larger inlet systems, we introduce a scale factor α, which is essentially a multiplier of the surface area of small tidal inlets. Thus, $\alpha = 2$ represents medium-sized inlet systems (with $100 < A_B < 200\ km^2$), and α = 4 represents large inlet systems (with $200 < A_B < 400\ km^2$). Note that the medium and large tidal inlet classes here are based on the estuary data base used by Bamunawala et al.[21]. Using the empirical relationships defining morphological equilibrium and assuming that the tidal range remains unchanged, the key terms in the above equations can now be expressed in terms of α as below:

Basin area $A_B \sim \alpha$; equilibrium basin volume $V_e \sim \alpha^{3/2}$, inlet cross-sectional area $A_c \sim \alpha$; distance $L \sim \alpha^{1/2}$, horizontal exchange coefficient $\delta \sim \alpha^{1/2}$, and morphological time scale $T \sim \left(\alpha^{1/2} + \alpha\right)/2$.

Substituting for the various terms in terms of the above α quantities, and assuming $\Delta S = R_2 t_2$, [9] can be re-arranged as:

$$M = 1 + \frac{1}{G}\left[e^{-G} - 1\right] \tag{11}$$

where, $G = T^{-1} \sim 2/\left(\alpha^{1/2} + \alpha\right)$.

Using [11] with α = 1, 2, and 4, the following M values are obtained for small, medium, and large tidal-inlet systems:

M ~ 0.5 for Small tidal inlets with $\alpha = 1$,
M ~ 0.25 for Medium-sized tidal inlets with $\alpha = 2$, and.
M ~ 0.15 for Large tidal inlets with $\alpha = 4$.

G-SMIC model description

G-SMIC is a fully probabilistic, reduced complexity model that computes sediment exchange between the nearshore and the estuary and resulting shoreline evolution at ~ 100 year time scales. The model has been validated against satellite-derived shoreline change estimates at more than 10 catchment-estuary-coast systems around the world[9,21]. G-SMIC is fully described in Bamunawala et al.[8,9], and hence, only a brief description is given here.

The main governing equation of *G-SMIC* is:

$$\Delta V_T = \Delta V_{BI} + \Delta V_{BV} + \Delta V_{FS} \tag{12}$$

where, ΔV_T is the cumulative change in the total sediment-volume exchange between the estuary and the adjacent coast, ΔV_{BI} is the basin infilling due to increases in basin accommodation space (driven by sea-level rise), ΔV_{BV} is the change in basin infill sediment volume due to variations in river discharge, and ΔV_{FS} is the change in fluvial sediment supply due to combined effects of climate change and anthropogenic activities (all volumes in m^3).

The different terms in [12] are computed as below:

$$\Delta V_{BI} = -M\left(A_B \Delta S\right) \tag{13}$$

where, A_B is the basin surface area (m^2), M ($0 < M < 1$) is the basin infilling lag factor, and ΔS is the sea-level rise.

$$\Delta V_{BV} = \frac{\Delta Q_R V_B}{(P + Q_R)} \tag{14}$$

where, Q_R is the present river flow into the basin during ebb, ΔQ_R is the climate change-driven variation in river flow during ebb, V_B is the present basin volume, and P is the mean equilibrium ebb-tidal prism (all volumes in m^3).

In *G-SMIC*, the change in fluvial sediment supply (ΔV_{FS} (m^3)) is calculated using the BQART model presented by Syvitski and Milliman[30] expressed as:

$$Q_S = \omega B Q^{0.31} A^{0.5} R_c T_c \tag{15}$$

where, ω is a coefficient equal to 0.02 or 0.0006 for the annual fluvial sediment supply (Q_S), expressed in kg/s or MT/year at catchments with its mean annual temperature greater than 2 ℃, Q is the annual cumulative river discharge (km^3), A is the river catchment area (km^2), R_c is catchment relief (km), and T_c is the catchment-wide mean annual temperature (℃).

The term 'B' in [15] represents the catchment sediment production, given by [16]:

$$B = IL_c\,(1 - T_E)\,E_h \tag{16}$$

where, L_c is the lithology factor that represents the catchment's soil type and erodibility, T_E is the catchment-wide reservoir trapping efficiency factor, and E_h is the human-induced erosion factor of the river catchment, which here is represented by the human footprint index (HFPI)[31,32].

The term I in [16] is the glacial erosion factor, which is given by:

$$I = 1 + (0.09A_g) \tag{17}$$

where, A_g is the ice cover percentage within the catchment area.

As previous studies (e.g., Wright and Nittrouer[33]) have shown that sediment loads projected by the BQART model consist mostly of suspended sediment, which is likely to be lost to the sea without contributing to a change in beach volume, in *G-SMIC*, a stochastic factor (fac_Q_s) is used when using BQART[21]. Thus, coastal sediment budget computations consider only a fraction of the fluvial sediment load.

G-SMIC requires four stochastic inputs: (1) annual mean temperature (T_c), (2) annual cumulative runoff (Q), (3) change in global mean sea level (ΔS), and (4) human-induced erosion factor (E_h). With these stochastic inputs, a Monte-Carlo simulation is implemented to probabilistically determine the change in total sediment volume exchange (ΔV_T) between the inlet system and adjacent inlet-interrupted coasts.

To derive shoreline change-projections, the 10th, 50th, and 90th percentiles of the annual ΔV_T are used to compute consequent shoreline change. Following the approach adopted by Ranasinghe et al.[11], the total sediment volume change is assumed to shift the active coastal profile forward or backward along the inlet-affected coast, thereby moving the shoreline forward (i.e., progradation) or backward (i.e., retreat). Note that this study assesses only the shoreline change due to ΔV_T. To assess the "total" amount of climate change driven shoreline change, this estimate could be combined with that due to the Bruun effect (for instance using the modified Bruun rule presented by Vousdoukas et al.[34]).

Model inputs

Catchment wide mean annual temperature and annual cumulative runoff values are obtained from four IPCC CMIP6 GCMs (viz., BCC-CSM2-MR, CESM2, CNRM-CM6-1-HR, and GFDL-ESM4). The global projections (5th, 50th, and 95th percentile) from NASA were used to generate stochastic variables of SLR[29,35,36]. The basin volumes were estimated via the linear regression model used in the global application of *G-SMIC*[21]. The basin surface-area values are obtained from the DIVA dataset[37]. The river network and basin information given by Lehner et al.[38] was used to determine the river catchment areas of the selected inlet-estuary systems. The global estimates of active profile slopes presented by Athanasiou et al.[39] are used in this study to obtain the depth of closure values. The catchment relief and reference HFPI values were extracted from one arc-second resolution digital elevation model (DEM) from the USGS earth explorer tool[40] and human footprint index (HFPI) data presented by Venter et al.[31,32], respectively.

Model applications

G-SMIC is here applied at the three selected tidal inlet systems representing small, medium, and large systems (as defined above) under for IPCC AR6 climate scenarios (SSP1-2.6, SSP2-4.5, SSP3-7.0 and SSP5-8.5). All simulations span the period 2030 (taken here as present-day) to 2100. The key system characteristics are shown in Table 1 above.

Data availability

The data supporting the calculation and conclusions presented in this manuscript will be made available by the corresponding author, without reservation, to any qualified researcher.

Received: 15 April 2024; Accepted: 11 January 2025
Published online: 04 February 2025

References

1. Aubrey, D. G. & Weishar, L. *Hydrodynamics and Sediment Dynamics of Tidal Inlets* (Springer, 1988).
2. Kjerfve, B. *Coastal Lagoon Processes* (Elsevier Science, 1994).
3. Davis-Jr, R. A. & Fitzgerald, D. M. *Beaches and Coasts* (Wiley, 2003).
4. Woodroffe, C. D. *Coasts: Form, Process and Evolution* (Cambridge University Press, 2003).

5. FitzGerald, D., Georgiou, I. & Miner, M. Estuaries and tidal inlets. In *Coastal Environments and Global Change* (eds Masselink, G. & Gehrels, R.) (John Wiley & Sons, Ltd, 2015).
6. Duong, T. M., Ranasinghe, R., Walstra, D. & Roelvink, D. Assessing climate change impacts on the stability of small tidal inlet systems: Why and how?. *Earth Sci. Rev.* **154**, 369–380 (2016).
7. McSweeney, S. L., Kennedy, D. M., Rutherfurd, I. D. & Stout, J. C. Intermittently closed/open lakes and lagoons: Their global distribution and boundary conditions. *Geomorphology* **292**, 142–152 (2017).
8. Bamunawala, J. et al. A holistic modeling approach to project the evolution of inlet-interrupted coastlines over the 21st century. *Front. Mar. Sci.* https://doi.org/10.3389/fmars.2020.00542 (2020).
9. Bamunawala, J. et al. Probabilistic application of an integrated catchment-estuary-coastal system model to assess the evolution of inlet-interrupted coasts over the 21st century. *Front. Mar. Sci.* **7**, 1104 (2020).
10. Nicholls, R.J., P.P. Wong, V.R. Burkett, J.O. Codignotto, J.E. Hay, R.F. McLean, S. Ragoonaden and C.D. Woodroffe, 2007: Coastal systems and low-lying areas. Climate Change 2007: Impacts, Adaptation and Vulnerability. Contribution of Working Group II to the Fourth Assessment Report of the Intergovernmental Panel on Climate Change, M.L. Parry, O.F. Canziani, J.P. Palutikof, P.J. van der Linden and C.E. Hanson, Eds., Cambridge University Press, Cambridge, UK, 315-356.
11. Ranasinghe, R., Duong, T. M., Uhlenbrook, S., Roelvink, D. & Stive, M. Climate-change impact assessment for inlet-interrupted coastlines. *Nat. Clim. Chang.* **3**, 83–87 (2013).
12. Toimil, A. et al. Climate change-driven coastal erosion modelling in temperate sandy beaches: Methods and uncertainty treatment. *Earth Sci. Rev.* **202**, 103110 (2020).
13. Duong, T. M., Ranasinghe, R. & Callaghan, D. P. Probabilistic projections of the stability of small tidal inlets at century time scale using a reduced complexity approach. *Sci. Rep.* **11**, 22921 (2021).
14. Duong, T. M. Climate change induced coastline change adjacent to small tidal inlets. *Front. Mar. Sci.* https://doi.org/10.3389/fmars.2021.754756 (2021).
15. Samaras, A. G. Towards integrated modelling of watershed-coast system morphodynamics in a changing climate: A critical review and the path forward. *Sci. Total Environ.* **882**, 163625 (2023).
16. Dissanayake, D. M. P. K., Ranasinghe, R. & Roelvink, J. A. The morphological response of large tidal inlet/basin systems to relative sea level rise. *Clim. Change* **113**, 253–276 (2012).
17. van der Wegen, M. Numerical modeling of the impact of sea level rise on tidal basin morphodynamics. *J. Geophys. Res. Earth Surf.* **118**, 447–460 (2013).
18. van der Wegen, M., Jaffe, B., Foxgrover, A. & Roelvink, D. Mudflat morphodynamics and the impact of sea level rise in South San Francisco Bay. *Estuar. Coasts* **40**, 37–49 (2017).
19. Besset, M., Anthony, E. J. & Bouchette, F. Multi-decadal variations in delta shorelines and their relationship to river sediment supply: An assessment and review. *Earth Sci. Rev.* **193**, 199–219 (2019).
20. Duong, T. M. et al. Assessing climate change impacts on the stability of small tidal inlets: Part 2—Data rich environments. *Mar. Geol.* **395**, 65–81 (2018).
21. Bamunawala, J. et al. Twenty-first-century projections of shoreline change along inlet-interrupted coastlines. *Sci. Rep.* https://doi.org/10.1038/s41598-021-93221-9 (2021).
22. Bruneau, N. et al. Future evolution of a tidal inlet due to changes in wave climate, Sea level and lagoon morphology (Óbidos lagoon, Portugal). *Cont. Shelf Res.* **31**, 1915–1930 (2011).
23. Stive, M. J. F. & Wang, Z. B. Chapter 13 morphodynamic modeling of tidal basins and coastal inlets. In *Advances in Coastal Modeling* (eds Stive, M. J. F. & Wang, Z. B.) (Elsevier, 2003).
24. Stive, M., Wang, Z., Ruol, P., & Buijsman, M. Morphodynamics of a tidal lagoon and adjacent coast. in *8th International Biennial Conference on Physics of Estuaries and coastal Seas* (The Hague, The Netherlands, 1998).
25. Van Goor, M. A., Zitman, T. J., Wang, Z. B. & Stive, M. J. F. Impact of sea-level rise on the morphological equilibrium state of tidal inlets. *Mar. Geol.* **202**, 211–227 (2003).
26. FitzGerald, D. M., Fenster, M. S., Argow, B. A. & Buynevich, I. V. Coastal impacts due to sea-level rise. *Annu. Rev. Earth Planet. Sci.* **36**, 601–647 (2008).
27. Leuven, J. R. F. W., Pierik, H. J., van der Vegt, M., Bouma, T. J. & Kleinhans, M. G. Sea-level-rise-induced threats depend on the size of tide-influenced estuaries worldwide. *Nat. Clim. Chang.* **9**, 986–992 (2019).
28. Bruun, P. Sea-level rise as a cause of shore erosion. *J. Waterw. Harb. Div. Proc. Am. Soc. Civ. Eng.* **88**, 117–130 (1962).
29. Fox-Kemper, B. et al. Ocean, cryosphere and sea level change. In *Climate Change 2021: The Physical Science Basis. Contribution of Working Group I to the Sixth Assessment Report of the Intergovernmental Panel on Climate Change* (eds Masson-Delmotte, V. et al.) (Cambridge University Press, 2021).
30. Syvitski, J. P. M. & Milliman, J. D. Geology, geography, and humans battle for dominance over the delivery of fluvial sediment to the coastal ocean. *J. Geol.* **115**, 1–19 (2007).
31. Venter, O. et al. Sixteen years of change in the global terrestrial human footprint and implications for biodiversity conservation. *Nat. Commun.* **7**, 12558 (2016).
32. Venter, O. *et al. Last of the Wild Project, Version 3 (LWP-3): 2009 Human Footprint, 2018 Release*. (Palisades, New York: NASA Socioeconomic Data and Applications Center (SEDAC), 2018). https://doi.org/10.7927/H46T0JQ4 (accessed 01 Mar 2023).
33. Wright, L. D. & Nittrouer, C. A. Dispersal of river sediments in coastal seas: Six contrasting cases. *Estuaries* **18**, 494 (1995).
34. Vousdoukas, M. I. et al. Sandy coastlines under threat of erosion. *Nat. Clim. Chang.* **10**, 260–263 (2020).
35. Garner, G. G. *et al. IPCC AR6 Sea Level Projections. Version 20210809*. https://doi.org/10.5281/zenodo.5914709 (2021).
36. Kopp, R. E. et al. The Framework for Assessing Changes To Sea-Level (FACTS) v1.0: A platform for characterizing parametric and structural uncertainty in future global, relative, and extreme sea-level change. *Geoscientific Model Development*, **16**, 7461–7489. https://doi.org/10.5194/gmd-16-7461-2023 (2023).
37. Hinkel, J. et al. A global analysis of erosion of sandy beaches and sea-level rise: An application of DIVA. *Glob. Planet. Chang.* **111**, 150–158 (2013).
38. Lehner, B., Verdin, K. & Jarvis, A. New global hydrography derived from spaceborne elevation data. *Eos Trans. Am. Geophys. Union* **89**, 93–94 (2008).
39. Athanasiou, P. et al. Global distribution of nearshore slopes with implications for coastal retreat. *Earth Syst. Sci. Data* **11**, 1515–1529 (2019).
40. Farr, T. G. et al. The shuttle radar topography mission. *Rev. Geophys.* https://doi.org/10.1029/2005RG000183 (2007).

Acknowledgements

The authors wish to thank the SLR projection authors for developing and making the projections available and the NASA Sea Level Change Team for developing and hosting the IPCC AR6 Sea Level Projection Tool. RR is partially supported by the AXA Research fund.

Author contributions

RR and TMD conceptualised the study. ZW and RR developed the analytical solution for the basin-infilling lag factor *M*. JB performed all G-SMIC simulations with strategic guidance from RR. RR and JB wrote the first complete draft of the manuscript. All authors contributed to refining the manuscript.

Declarations

Competing interests

The authors declare no competing interests.

Additional information

Supplementary Information The online version contains supplementary material available at https://doi.org/10.1038/s41598-025-86699-0.

Correspondence and requests for materials should be addressed to R.R.

Reprints and permissions information is available at www.nature.com/reprints.

Publisher's note Springer Nature remains neutral with regard to jurisdictional claims in published maps and institutional affiliations.